Journal of Molecular Structure 1245 (2021) 131031

Contents lists available at ScienceDirect

Journal of Molecular Structure

journal homepage: www.elsevier.com/locate/molstr

Supramolecular, spectroscopic and computational analysis of weak interactions in some thiosemicarbazones derived from 5-acetylbarbituric acid

Alfonso Castiñeiras[a,1,2,*], Nuria Fernández-Hermida[a], Isabel García-Santos[a], Lourdes Gómez-Rodríguez[a], Diego M. Gil[b], Antonio Frontera[c]

[a] Department of Inorganic Chemistry, Faculty of Pharmacy, University of Santiago de Compostela, 15782-Santiago de Compostela (Galicia), Spain
[b] INBIOFAL (CONICET-UNT). Instituto de Química Orgánica. Facultad de Bioquímica, Química y Farmacia, Ayacucho 471, T4000INI San Miguel de Tucumán, Argentina
[c] Departament de Química, Universitat de les Illes Balears, Ctra. de Valldemossa km 7.5, 07122-Palma de Mallorca (Baleares), Spain

ARTICLE INFO

Article history:
Received 23 April 2021
Revised 21 June 2021
Accepted 2 July 2021
Available online 19 July 2021

Keywords:
Thiosemicarbazones
5-acetylbarbituric acid
Heterocycles
Crystal structure
Hirshfeld surface
DFT calculations

ABSTRACT

A new series of 5-acetylbarbituric based thiosemicarbazones (TSC) named 5-acetylbarbituric hydrazine-1-carbothioamide (**1**), N-methyl-(5-acetylbarbituric)hydrazine-1-carbothioamide (**2**), N-ethyl-(5-acetylbarbituric)hydrazine-1-carbothioamide (**3**), N,N-dimethyl-(5-acetylbarbituric)hydrazine-1-carbothioamide (**4**), N'-piperidine-(5-acetylbarbituric)-1-carbothiohydrazide (**5**) and N'-hexamethyleneimine-(5-acetylbarbituric)-1-carbothiohydrazide (**6**), has been synthesized from 5-acetylbarbituric acid and N-unsubstituted/substituted thiosemicarbazides. The synthesized compounds were well characterized by elemental analyses, FT-IR, ^{1}H, ^{13}C NMR and mass spectroscopic methods. Three-dimensional molecular structures of three compounds (**1**·DMSO, **2** and **6**·H_2O) were determined by single crystal X-ray crystallography, and an analysis of their supramolecular structure was carried out. The supramolecular features of the X-ray structure were also studied using Hirshfeld surface analysis. Finally, H-bonding networks observed in the solid state X-ray structures of **1**·DMSO, **2**, and **6**·H_2O and unconventional π-stacking dimers in **6**·H_2O were further analyzed by DFT calculations in combination with molecular electrostatic potential surfaces and combined QTAIM/NCIplot computational tools.

1. Introduction

The use of thiosemicarbazides or thiosemicarbazones (TSC) in organic synthesis has become a classic strategy for the preparation of different heterocycles. Many researchers have reported S/N regioselective nucleophilic competition in the synthesis of heterocyclic compounds by intramolecular cyclization reactions. Changes in reaction conditions can induce an S or an N attack to eventually provide different cyclic products from a single starting material [1]. Also, TSC are a type of ligand that has considerable interest for medicinal chemists due to their therapeutic potential. It is believed that the presence of the sulfur atom and its ability to bind to metals in the biological system is the main reason for their biological activities, such as anticancer, antitumor, antifungal, antibacterial, antimalarial, antiviral and anti-HIV, and their mechanism of action probably involves the inhibition of ribonucleotide reductase, converting ribonucleotides into deoxyribonucleotides. Furthermore, TSC that have an aromatic heterocyclic moiety appear to have improved biological activities [2]. In general, TSC are easy to synthesize and their structure can be modified in multiple ways. In some cases, small modifications result in dramatic changes to the chemistry which bring about a rational design of their metal complex stability, redox potentials, membrane permeability and, ultimately, biological activity. A condensation reaction between a thiosemicarbazide and an aldehyde or ketone gives a thiosemicarbazone [3]. Alternatively, reactions between the methyl ester of imidopicolinic acid and thiosemicarbazides also result in TSC [4].

Furthermore, the medical importance of many pyrimidine derivatives is significant since they have antineoplastic, antiviral, antibiotic, and anti-inflammatory properties, among other biolog-

* Corresponding author at: Universidad de Santiago de Compostela, Facultad de Farmacia, Campus Universitario sur, E-15782 Santiago de Compostela, Spain.
E-mail address: alfonso.castineiras@usc.es (A. Castiñeiras).
[1] URL: http://www.usc.es/giqimo/.
[2] ORCID ID: https://orcid.org/0000-0002-5070-5936.

https://doi.org/10.1016/j.molstruc.2021.131031

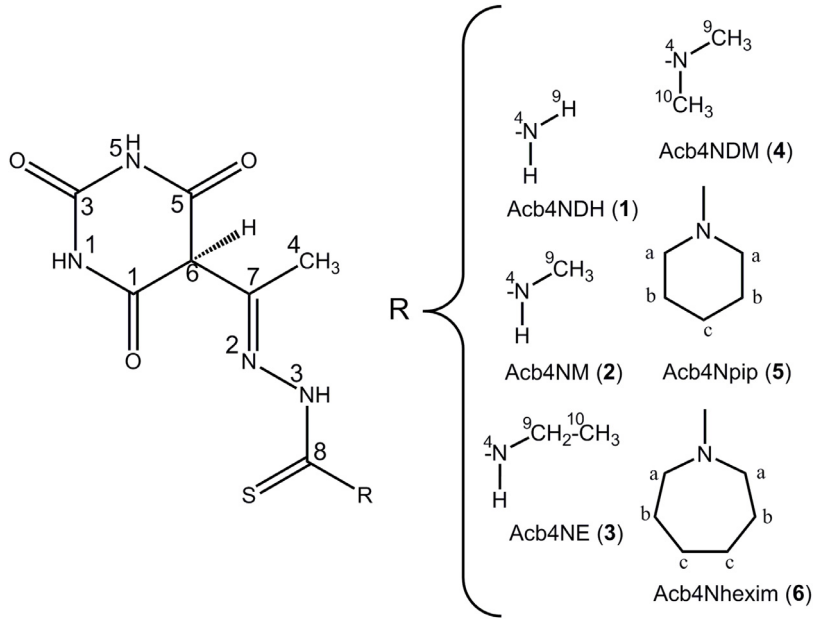

Chart 1. Synthesized thiosemicarbazones derived from 5-acetylbarbituric acid with atoms labelling for NMR analysis.

ical activities. Many synthetic molecules containing pyrimidine, such as certain barbituric acid derivatives or sulfadiazine, are also important as synthetic drugs and chemotherapeutic agents, and have been developed using the small 5-acylbarbiturate moieties as the main building block in their preparation [5].

So, in light of the above regarding TSC and barbituric acid derivatives, it is likely that the combination of both types of compounds may lead to new biologically active agents. Consequently, we have carried out the reaction between such bioactive moieties, as already tested in previous works [1,6]. In this work we present the synthesis of some new thiosemicarbazone derivatives (Chart 1) via the condensation of 5-acetylbarbituric acid and N-unsubstituted/substituted thiosemicarbazides. All the structures of the newly synthesized materials were confirmed by both elemental and spectral (FT-IR, ^{1}H, ^{13}C NMR and mass) tools. The crystal and molecular structures of three TSC and of 5-(5-methyl-2-(methylcarbamothioyl)-3-oxo-2,3-dihydro-1H-pyrazol-4-yl)-2-(methylamino)-1,3,4-thiadiazol-3-ium ethyl sulfate, obtained serendipitously, were determined by the X-ray diffraction of single-crystals. The supramolecular assemblies observed in the solid state focusing on the H-bonding networks and π-stacking interactions were analyzed by Hirshfeld surface analysis and DFT calculations in combination with MEP, QTAIM and NCIplot computational tools.

2. Experimental

2.1. Materials and physical measurements

All reagents and solvents were commercial products that were used as received, without further purification. Melting points were determined on a Büchi melting point apparatus and are uncorrected. Mass spectra were obtained on a Micromass AUTOAPEC spectrometer for ESI (Supplementary material, Figures S1-S6). Microanalyses (C, H and N) were carried out using a Carlo-Erba 1108 elemental analyser. FT-IR spectra were recorded from KBr pellets over the range 4000-400 cm^{-1} on a Bruker IFS-66v spectrometer. ^{1}H and ^{13}C NMR spectra in DMSO-d$_6$ were run on Bruker AMX 300 and WM 300 instruments, respectively, using TMS as an internal reference.

2.2. Synthesis of 5-Acetylbarbituric acid and thiosemicarbazones

5-Acetylbarbituric acid (5Acba) was prepared according to literature procedure [7]. The TSC were prepared by condensation reactions between 5-Acb and the unsubstituted/substituted thiosemicarbazides [1,6], as follows (Scheme 1): a mixture of 5Acba (0.01 mole) and of the corresponding thiosemicarbazide (0.01 mole) in 96% ethyl alcohol (45 mL) with 2 drops of conc. H_2SO_4 was heated under reflux for 2 hours, cooled, and stirred for 3 days at room temperature. The precipitate was filtered off and recrystallized from ethanol.

2.3. Synthesis of 5-acetylbarbituric hydrazine-1-carbothioamide (*1*)

Colourless solid, 80.9% yield; m.p. 270°C to 272°C. MS m/z, (%): 243 (M^{+}, 2). Anal. Calc. for $C_7H_9N_5O_3S$ (243.24): C, 34.6; H, 3.7; N, 28.8; S, 13.2. Found: C, 34.9; H, 3.7; N, 28.0; S, 12.9%. IR (KBr, ν/cm^{-1}): 3430s, 3297m, 3211s,br, 3104m, ν(N–H), 1725s ν(C=O), 1664s δ(NH), 1627s,br, 1553s [ν(C=N)+ν(C=C)], 1377m, 1282s, 1239s [ν(C=S)+ν(C=N)], 1039m ν(N–N), 830w ν(C=S). ^{1}H NMR (DMSO-d$_6$, δ/ppm): 2.6 (3H, Me), 8.1 (2H, N4H2), 10.1 (1H, N3H), 10.8 (1H, N1H), 10.6 (1H, N5H), 13.0 (1H, N2H). ^{13}C NMR (DMSO-d$_6$, δ/ppm): 15.7 (C-4), 88.8 (C-6), 149.6 (C-3), 167.9 (C-7), 174.0 (C-1, C-5), 181.0 (C-8).

Suitable crystals for X-ray diffraction were grown at room temperature as **1**·DMSO, after two weeks, from solutions prepared for NMR studies.

2.4. Synthesis of N-methyl-(5-acetylbarbituric)hydrazine-1-carbothioamide (*2*)

Colourless solid, 78.4% yield; m.p. 260°C to 262°C. MS m/z, (%): 257 (M^{+}, 24). Anal. Calc. for $C_8H_{11}N_5O_3S$ (257.27): C, 37.3; H, 4.3; N, 27.2; S, 12.5. Found: C, 37.8; H, 4.4; N, 26.9; S, 12.1%. IR (KBr, ν/cm^{-1}): 3329m, 3184m, 3211m, 3066m, ν(N–H), 1718s ν(C=O), 1655w δ(NH), 1633s,br, 1575s, 1517m [ν(C=N)+ν(C=C)], 1382m, 1362m, 1296m, 1236m [ν(C=S)+ν(C=N)], 1047w ν(N–N), 831m ν(C=S). ^{1}H NMR (DMSO-d$_6$, δ/ppm): 2.5 (3H, Me), 2.9 (3H, N4CH3), 8.3 (1H, N4H), 9.9 (1H, N3H), 10.8 (1H, N1H), 10.7 (1H, N5H), 13.1 (1H, N2H). ^{13}C NMR (DMSO-d$_6$, δ/ppm): 14.1 (C-9), 15.8

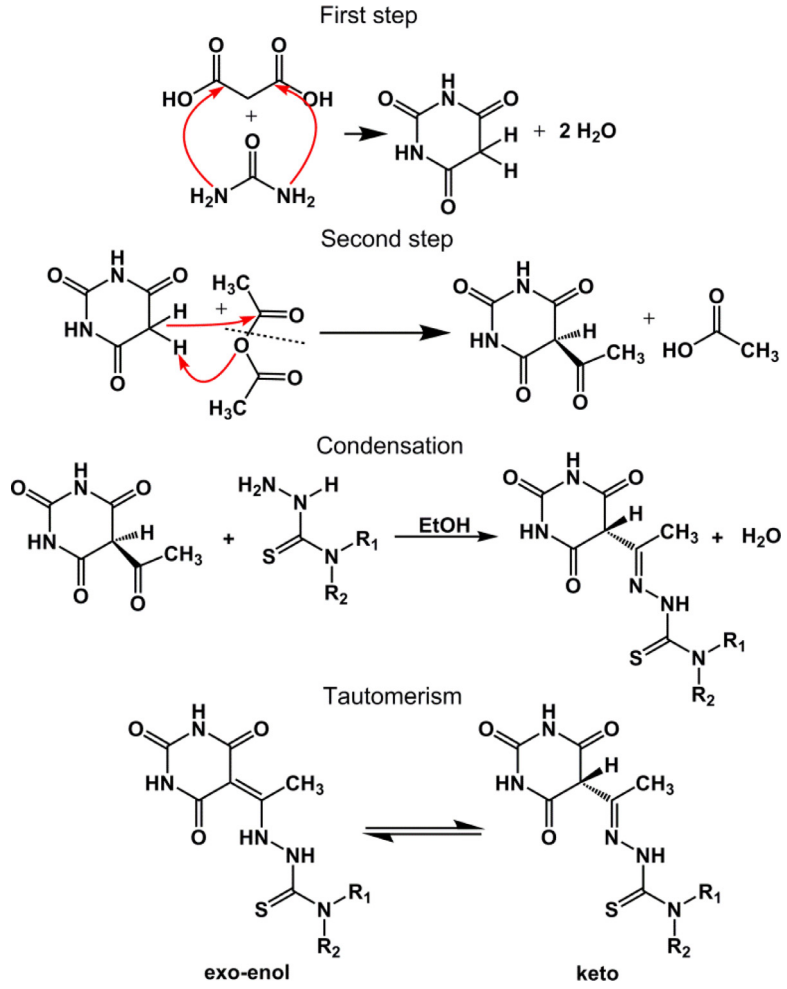

Scheme 1. Synthesis pathway of 5-acetylbarbituric acid and thiosemicarbazones, and general tautomeric behaviour of 5-acetylbarbituratethiosemicarbazones.

(C-4), 89.6. (C-6), 167.5 (C-7), 149.6 (C-3), 174.1 (C-1, C-5), 181.0 (C-8).

Suitable crystals for X-ray diffraction were grown as (**2**), after a short time, from the mother liquors.

*2.5. Synthesis of N-ethyl-(5-acetylbarbituric)hydrazine-1-carbothioamide (**3**)*

Colourless solid, 78.4% yield; m.p. 270°C to 272°C. MS m/z, (%): 271 (M^+, 3). Anal. Calc. for $C_9H_{13}N_5O_3S$ (271.29): C, 39.9; H, 4.8; N, 25.8; S, 11.8. Found: C, 40.1; H, 4.7; N, 25.6; S, 11.2%. IR (KBr, ν/cm^{-1}): 3329m, 3184m, 3111w, 3066w, ν(N–H), 1701s ν(C=O), 1659s δ(NH), 1572s, 1550s [ν(C=N)+ν(C=C)], 1298w, 1272m [ν(C=S)+ν(C=N)], 1051wm ν(N–N), 802m ν(C=S). ^{1}H NMR (DMSO-d$_6$, δ/ppm): 1.1 (3H, N4CH3), 2.5 (3H, Me), 3.4(2H, N4CH2), 8.4 (1H, N4H), 9.9 (1H, N3H), 10.6 (1H, N5H), 10.8 (1H, N1H), 13.1 (1H, N2H). ^{13}C NMR (DMSO-d$_6$, δ/ppm): 14.1 (C-10), 15.8 (C-4), -(C-9), 89.6 (C-6), 167.5 (C-7), 149.6 (C-3), 174.1 (C-1, C-5), 181.0 (C-8).

*2.6. Synthesis of N,N-dimethyl-(5-acetylbarbituric)hydrazine-1-carbothioamide (**4**)*

Yellow solid, 60.7% yield; m.p. 280°C to 282°C. MS m/z, (%): 271 (M^+, 36). Anal. Calc. for $C_9H_{13}N_5O_3S$ (271.29): C, 39.9; H, 4.8; N, 25.8; S, 11.8. Found: C, 39.9; H, 4.7; N, 25.5; S, 11.7%. IR (KBr, ν/cm^{-1}): 3380m,br, 3172m, 3106w, ν(N–H), 1728s ν(C=O), 1664s δ(NH), 1617s, 1577s, 1530s, [ν(C=N)+ν(C=C)], 1375s, 1318s, 1235m [ν(C=S)+ν(C=N)], 1069w ν(N–N), 839m ν(C=S). 1H NMR (DMSO-d6, δ/ppm): 2.5 (1H, C6H), 2.6 (3H, Me), 3.1 (6H, N4Me2), 10.5 (1H, N1H), 10.5 (1H, N5H), 13.5 (1H, N2H). 13C NMR (DMSO-d6, δ/ppm): 16.3 (C-4), 40.6 (C-9, C10), 88.3 (C-6), 150.0 (C-3), 165.9 (C-7), 171.3 (C-1, C-5), 181.4 (C-8).

*2.7. Synthesis of N'-piperidine-(5-acetylbarbituric)-1-carbothiohydrazide (**5**)*

Beige solid, 75.8% yield; m.p. > 300°C. MS m/z, (%): 226 ([$C_7H_6O_3N_4S$]$^+$, 39). Anal. Calc. for $C_{12}H_{17}N_5O_3S$ (311.36): C, 46.3; H, 5.5; N, 22.5; S, 10.3. Found: C, 45.8; H, 5.5; N, 22.0; S, 9.8%. IR (KBr, ν/cm^{-1}): 3341m,br, 3183m,br, 3111m, ν(N–H), 1718s ν(C=O), 1675s δ(NH), 1636s, 1577s, 1512s, [ν(C=N)+ν(C=C)], 1380m, 1357m, 1302m, 1273m, 1248m [ν(C=S)+ν(C=N)], 1041w ν(N–N), 831m ν(C=S). ^{1}H NMR (DMSO-d$_6$, δ/ppm): 1.6 (Hc), 1.6 (Hb), 2.5 (1H, C6H), 2.6 (3H, Me), 3.8 (Ha), 10.5 (1H, N1H), 10.5 (1H, N5H), 13.6 (1H, N2H). ^{13}C NMR (DMSO-d$_6$, δ/ppm): 16.17 (C-4), 23.8 (Cc), 25.4 (Cb). 49.1 (Ca), 87.9 (C-6), 149.8 (C-3), 170.1 (C-7), 174.1 (C-1, C-5), 180.1 (C-8).

*2.8. Synthesis of N'-hexamethyleneimine-(5-acetylbarbituric)-1-carbothiohydrazide (**6**)*

Colourless solid, 68.8% yield; m.p. > 300°C. MS m/z, (%): 198 ([$C_7H_{10}O_3N_4$]$^+$, 23). Anal. Calc. for $C_{13}H_{19}N_5O_3S$ (243.24): C, 48.0; H, 5.9; N, 21.5; S, 9.8. Found: C, 48.0; H, 5.7; N, 21.5; S, 9.5%. IR (KBr, ν/cm^{-1}): 3338m, 3178m,br, 3019m, ν(N–H), 1728s ν(C=O),

Table 1
Crystal data and structure refinement for **1**·DMSO, **2** and **6**·H_2O

Compound	**1**·DMSO	**2**	**6**·H_2O
Empirical formula	$C_9H_{15}N_5O_4S_2$	$C_8H_{11}N_5O_3S$	$C_{13}H_{21}N_5O_4S$
Formula weight	321.38	257.28	343.41
Temperature/K	293(2)	100(2)	100(2)
Wavelength/Å	1.54184	0.71073	0.71073
Crystal system	Triclinic	Monoclinic	Monoclinic
Space group	$P\bar{1}$	$P2_1/c$	$P2_1/n$
Unit cell dimensions			
a/Å	8.1322(3)	11.7397(5)	6.3848(10)
b/Å	8.9386(4)	6.7208(3)	28.301(6)
c/Å	10.0589(2)	13.9717(5)	8.7678(17)
α/°	78.839(3)	-	-
β/°	85.285(3)	106.404(2)	100.462(6)
γ/°	74.452(4)	-	-
Volume/Å^{-3}	690.75(4)	1057.50(8	1558.0(5)
Z	2	4	4
Calc. density/Mg/m^3	1.545	1.616	1.464
Absorp. coefc./mm^{-1}	3.718	0.313	0.237
F(000)	336	536	728
Crystal size/mm	0.32 × 0.24 × 0.12	0.23 × 0.10 × 0.03	0.19 × 0.04 × 0.02
θ range/°	4.483 - 69.955	1.808 - 25.340	1.439 - 21.966
Limiting indices/h,k,l	-9/9, 0/10, -12/12	-14/13, 0/8, 0/16	-6/6, 0/29, 0/9
Refl. collect/unique [R_{int}]	2790/2609 [0.0422]	19621/1930 [0.0480]	14672/1909 [0.0716]
Completeness θ/°, %	67.684, 100.0	25.242, 99.3	25.242, 67.8
Absorp. correct.	Psi-scan	Multi-scan	Multi-scan
Max. /min. transm.	1.000 - 0.576	1.000 - 0.913	1.0000 - 0.8528
Data/parameters	2609/217	1930/171	1909/226
Goodness-of-fit on F^2	1.022	1.065	1.021
Final R indices	$R_1 = 0.0490$, $wR_2 = 0.1341$	$R_1 = 0.0385$, $wR_2 = 0.1005$	$R_1 = 0.0541$, $wR_2 = 0.0976$
R indices (all data)	$R_1 = 0.0714$, $wR_2 = 0.1491$	$R_1 = 0.0504$, $wR_2 = 0.1084$	$R_1 = 0.1310$, $wR_2 = 0.1244$
Largest dif. peak/hole	0.394/-0.234	0.351/-0.388	0.338/-0.338
CCDC number	1961790	1961791	1961792

1623s δ(NH), 1578s, 1516sh [ν(C=N)+ν(C=C)], 1366m, 1316m, 1273m, 1241w [ν(C=S)+ν(C=N)], 1040w ν(N–N), 831w ν(C=S). ^{1}H NMR (DMSO-d_6, δ/ppm): 1.5 (Hb), 1.7 (Hc), 2.5 (1H, C6H), 2.5 (3H, Me), 3.9 (Ha), 10.8 (1H, N5H), 10.8 (1H, N1H), 13.5 (1H, N2H). ^{13}C NMR (DMSO-d_6, δ/ppm): 16.1 (C-4), 88.3 (C-6), 149.9 (C-3), 171.8 (C-7), 174.2 (C-1, C-5), 180.5 (C-8).

Crystals suitable for X-ray diffraction were grown as **6**·H_2O by slow evaporation of the mother liquors from the recrystallization after two weeks.

2.9. X-ray diffraction analysis

Diffraction data were obtained using an Enraf Nonius CAD4, an Enraf Nonius MACH3 or a Bruker X8 Kappa APEXII diffractometer from crystals mounted on glass fibers. Data were corrected for Lorentz and polarization effects and for absorption following psi-scan [8] or multi-scan [9] types. The structures were solved by direct methods [10] which revealed the positions of all non-hydrogen atoms. These were refined on F2 by a full-matrix least-squares procedure using anisotropic displacement parameters [10]. All hydrogen atoms were located on difference maps, and the positions of O–H and N–H hydrogen atoms were refined (others were included as riders); the isotropic displacement parameters of H atoms were constrained to 1.2/1.5 Ueq of the carrier atoms. Molecular graphics were generated using DIAMOND [11]. Crystal data, experimental details and refinement results are summarized in Table 1.

2.10. Theoretical methods

The Hirshfeld surfaces and their associated two-dimensional (2D) fingerprint plots [12-16] were generated using CrystalExplorer17.5 software [17] to visualize and quantify the various non-covalent interactions that are responsible for the crystal stabilization. The normalized contact distance (d_{norm}) is a symmetric function of distances to the surface from nuclei inside (d_i) and outside (d_e) the Hirshfeld surface, relative to their respective van der Waals (vdW) radii. Graphical plots of the Hirshfeld surfaces mapped with d_{norm} use a red-white-blue color scale, where red indicates shorter contacts, white is used for contacts around the vdW separation, and blue for longer contacts. The 3D d_{norm} surfaces were mapped over a fixed color scale of -0.075 au (red) to +0.75 au (blue). Hirshfeld surfaces of compounds **2** and **6** were also mapped with the shape index and curvedness properties (CPs).

The energetic features of the assemblies were computed using Gaussian-16 [18] at the PBE0-D3/def2-TZVP level of theory. The interaction energies were computed by calculating the difference between the energies of the isolated monomers and that of their assembly. These energies were corrected using the Boys and Bernardi counterpoise method [19]. Grimme's D3 dispersion correction has been used in the calculations [20]. To evaluate the interactions in the solid state, the crystallographic coordinates were used and only the position of the hydrogen bonds (HBs) has been optimized. This procedure and level of theory has been used before to investigate non-covalent interactions in the solid state [20-22]. The molecular electrostatic potential surfaces were computed at the same level and represented using the 0.001 a.u. isosurface. The QTAIM analysis [23] and NCIplot index [24] calculations were computed at the same level of theory by means of the AIMAll program [25].

3. Results and discussion

3.1. General comments on the synthesis

The 5Acba preparation is an acid-catalyzed one-pot three-component reaction between malonic acid, urea and acetic anhydride, constituting a relatively facile synthesis of the 5Acba. The first step in the mechanism is believed to be the condensation between the acid and urea to generate the cyclized product, 2,4,6-pyrimidinetrione, where the α-carbon has a reactive hydrogen atom and is quite acidic ($pK_a = 4.01$) because of the additional

aromatic stabilization of the carbanion. In a second step, the intermediate generated acts as an electrophile for the Friedel–Crafts acylation using acetic anhydride. As shown in Scheme 1, 5Acba in condensation with thiosemicarbazides, in the presence of concentrated sulfuric acid (a few drops), in absolute alcohol, produced N-(Substituted)-5-acetylbarbituric thiosemicarbazones **1**-**6**.

3.2. Vibrational spectroscopy

The infrared spectra of these compounds (Figures S7-S12 in Supporting Information file) showed characteristic absorption bands attributed to N-H, C=O and C=S bonds. The bands due to the stretching modes of the NH and NH_2 groups appear in the region 3000-3450 cm^{-1}, so that those with the highest frequency are due to the NH_2 group [26]. Therefore, if we compare the spectra of the synthesized TSC we observe that the band with the highest energy in **1** occurs at 3430 cm^{-1} and corresponds to $\nu_a(NH_2)$ [27] which is absent in the other TSC. Secondary thioamides have at strong band around 3200-3400 cm^{-1}, which sometimes appears as a double band due to the existence of cis-trans isomerism [28], although in condensed phases a single strong band is observed at around 3300 cm^{-1}. The ν(NH) band, which should be at around 1650 cm^{-1}, appears combined with the ν(C=O) bands. A band due to S-H stretching modes should appear in the 2550-2600 cm^{-1} region. The absence of such a band in the TSC spectra confirms the existence in the solid state of the tautomeric form tiona [29]. In the 1500-1600 cm^{-1} interval a band is observed and can be attributed to ν(CN + CC) but can also be due to a combination of ν(NH) and ν(CN) or even a combination of the three, so it is difficult to know exactly which assignment it corresponds to [30]. The band close to 800 cm^{-1} is assigned to the pure C=S stretching modes, while the one that appears at 1110-1075 cm^{-1} may be coupled with N-C-N vibrations. The complexity of the –C-N(H)-N(H)-C(=S)-NH_2 system makes it difficult to characterize this band. At around 1000 cm^{-1} a band corresponding to the N-N stretching modes is observed.

3.3. NMR spectroscopy

The compounds may exist in four tautomeric forms, [a-d], as shown in Chart 2. As occurs in Schiff bases derived from 2,4,6-pyrimidinetrione [31], the exchange of a proton brings about the possible existence in solution of two isomers, one with a carbon-carbon double bond (a) and the other with a carbon-nitrogen double bond (b). This equilibrium is sensitive to temperature so that, at room temperature, isomer (b) is the most abundant (approximately 90 %), in the solid state. However, in solution, if the solvent has a heat capacity high enough to overcome the high equilibrium activation energy, the amount of isomer (a) will increase significantly and may become the predominant form. This fact, together with the existence of keto-enolic equilibrium (a-d) (Chart 2) and the possible existence in solution of other typical isomers of this type of TSC [32], significantly complicates the interpretation of the ^{1}H NMR spectra.

The ^{1}H NMR spectra of the synthesized compounds (Figures S13-S18 in Supporting Information file) showed two characteristic signals in the δ range of 2.5 to 2.6 ppm and 13.0 to 13.6 ppm due to the C-CH_3 and N2H protons, respectively. In the spectrum of **1** and in those of the N-monosubstituted thiosemicarbazones (**2**-**3**), the protons of the 2,4,6-pyrimidinetrione ring, as occurs in the 5-acetylbarbituric acid spectrum [33], give rise to two different signals at 10.8 and 10.7 ppm, with the N1H proton being the least shielded. Furthermore, these spectra show a signal in the range of 9.9-10.1 ppm that is due to the N3H proton. In the spectra of the N-disubstituted thiosemicarbazones (**4**-**6**), a single signal appears between 10.4 and 10.8 ppm for the N1H and N5H protons, the signal due to the N3H proton is absent, and a new signal appears

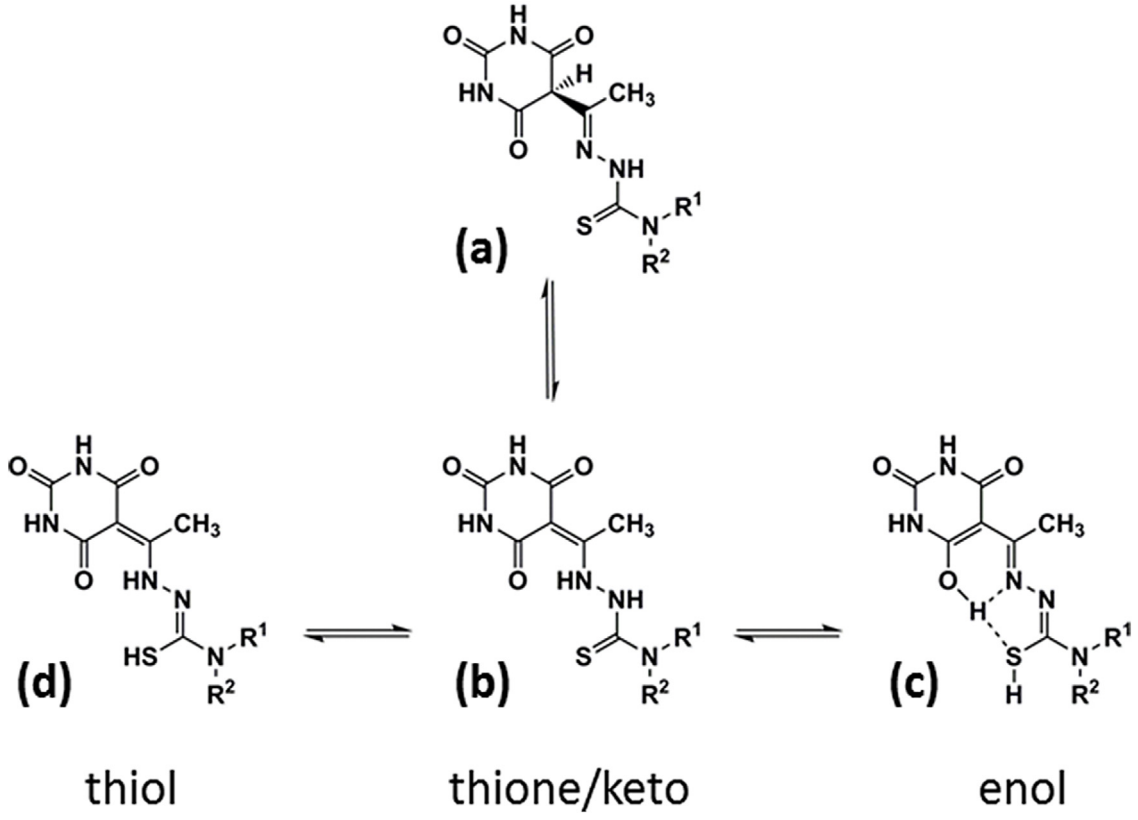

Chart 2. Tautomeric forms of 5-acetylbarbituric thiosemicarbazone derivatives.

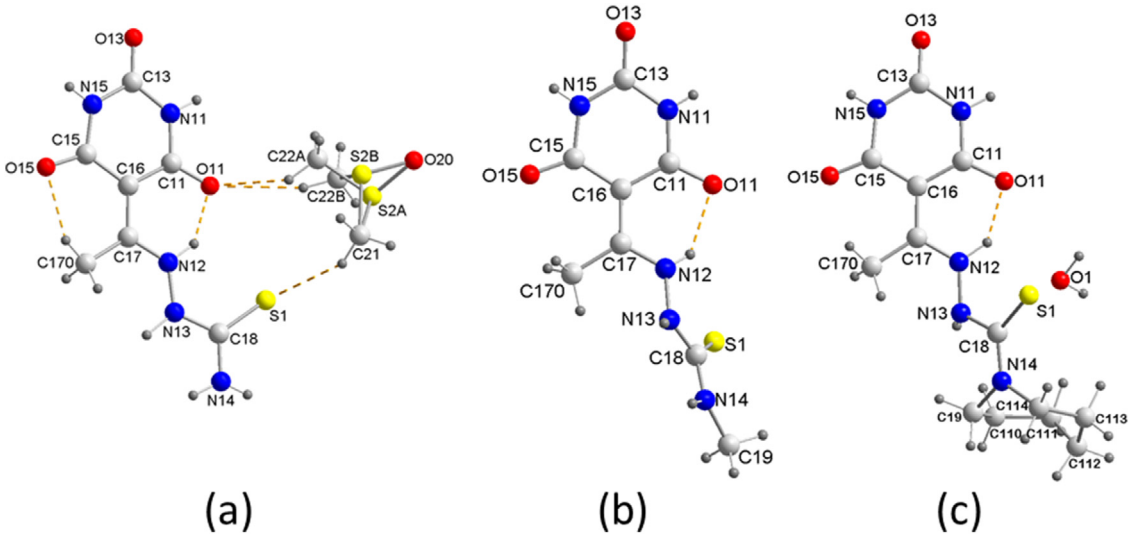

Fig. 1. Perspective view of: (a) **1**·DMSO, (b) **2** and (c) **6**·H_2O, showing the asymmetrical unit and the atom-numbering scheme. Hydrogen bonds are shown as orange dashed lines.

at 2.45 ppm which is attributed to the C6H proton on the 2,4,6-pyrimidinetrione ring (Chart 1). This fact reflects the keto/exo-enol tautomerism present in solution (Scheme 1).

To assign the signals of the ^{13}C NMR spectra (Figures S19-S24 in Supporting Information file), of 5-acetylbarbituric acid and those of different TSCs have been taken into account. In the acid spectrum, when the TSC is formed, it is observed that the signal corresponding to C3 is shifted upfield, due to the transformation of the carbonyl group into an azomethine group the shielding of the signal corresponding to C2 also takes place. In principle, because the form with the C2=C3 bond is predominant in the thiosemicarbazone, versus the form with the C3=N2 bond, one would expect the C2 signal to shift downfield. However, the less shielded effect of the C=N group compared to C=O causes an upfield shift.

Furthermore, due to the asymmetry of C2 in 5-acetylbarbituric acid, two different signals are observed for the C1 and C6 carbons. This asymmetry disappears when the TSC is formed, due to the greater stability of the form, and this means that, in the spectra of the latter, a single signal is observed for both atoms. In **2**, the presence of two different signals may be due to the E/Z isomerism around the C2=C3 bond or to the presence in solution of a certain amount of the b form [34]. The increase in electronic delocalization with the formation of TSCs also causes less shielding in the C1, C6 and C7 signals. As in other similar barbiturates, this shift in C1 and C6 is much greater than in C7. Furthermore, the signal corresponding to C4 (the carbon of the methyl group) shifts upfield due to the lower inductive effect of the C=N group compared to the C=O present in 5-acetylbarbituric acid. Finally, the signals around 150 and 170 ppm correspond to carbon atoms of the carbonyls of the 2,4,6-pyrimidinetrione moiety, and another, around 181 ppm to the carbon atom of thiocarbonyl.

3.4. Structural description and supramolecular analysis

Here we report on the crystal structure of three 5-acetylbarbituric thiosemicarbazone derivatives (**1**·DMSO, **2** and **6**·H_2O), that can exist in four tautomeric forms, giving rise to different molecular conformations and hydrogen bonding patterns. The asymmetric units are shown in Fig. 1. The bond lengths found in all three compounds (Table S1, in Supporting Information file) show significant uniformity in the moieties thiosemicarbazone, and indicate some electronic delocalization along the chain, extending up to the C16-C17 bond, although the greatest partial double bond character is concentrated in the C17-N12 and C18-S1 bonds, in contrast with the values found in other thiosemicarbazones, where a strong conjugation is observed in the C18-S1 and C18-N13 bonds [1,35]. As can be observed in Fig. 1a, in **1**·DMSO there is a disorder in the DMSO molecule that affects only the sulfur atom (S2) and the carbon atom of one of the methyl groups (C22). These atoms were refined using a split (S2A/S2B and C22A/C22B) with 50% occupancy for each position.

Although in the solid phase all three TSC are presented in the tautomeric form exo-enol (Chart 2), there are some differences between them with regard to the molecular conformation. The molecule of **1**·DMSO (Fig. 1a) is flat with a maximum deviation of its atoms from the least-squares plane of 0.054 Å (N15) and torsion angles of 0.2(4)° (N12-N13-C18-S1) and 179.3(3)° (N12-N13-C18-N14), while in **2** and **6**·H_2O (Fig. 1b and 1c, respectively) the 2,4,6-pyrimidinetrione and thiosemicarbazide planes are rotated with respect to each other forming a dihedral angle of 57.6(1)° and 46.7(2)°, respectively, and the N12-N13-C18-S1/N12-N13-C18-N14 torsion angles are −11.2(3)/169.6(2)° and 12.2(6)/171.9(4)°, in **2** and **6**·H_2O, respectively.

Moreover whereas in **1**·DMSO the N13 atom is contained in the plane formed by the atoms N12/H13/C18 [deviation 0.004(12) Å], in **2** and **6**·H_2O this atom is outside the referred plane [deviation −0.132(12) and 0.279(22) Å, respectively]. Both differences in the molecular structure of the three compounds may be related to their crystal packing. While the loss of planarity of the molecule in **2** and **6**·H_2O must be attributed to the influence of the substituent linked to the N14 atom, the decrease in sp^2 hybridization in N13 may be due to the participation of the N13−H13 bond in interactions of hydrogen bonding with the nearest neighbor molecules. The bond lengths and bond angles of the 2,4,6-pyrimidinetrione ring are in the allowed ranges for barbituric acid derivatives [36]. The molecular structure of **1**·DMSO was stabilized by N12−H12···O11 and C170−H17C···O15 intramolecular interactions which generated S(6) motifs, whereas the molecular structures of **2** and **6**·H_2O are stabilized only by N12−H12···O11 intramolecular interactions. From the point of view of classical hydrogen bonding, in **1**·DMSO, each TSC molecule contains three oxygen and one sulfur acceptor atoms, and six N-H donors, in addition to those of the DMSO molecule. In the crystal packing of **1**·DMSO there is an accessible void solvent of approximately 226

Table 2
Hydrogen bond parameters [Å, °] for **1**·DMSO, **2** and **6**·H_2O. The letters in brackets refer to the symmetry codes shown in the text and figures.

Comp.	D–H···A	D–H	H···A	D···A	∠DHA	Symmetry code
1•DMSO	N11–H11···O13[a]	0.85(4)	1.99(4)	2.841(3)	174(4)	-x+1,-y,-z+1
	N12–H12···O11	0.94(3)	1.70(3)	2.514(3)	143(3)	
	N13–H13···O20[b]	1.04(3)	1.75(3)	2.735(3)	156(3)	x,y,z-1
	N14–H14A···O20[b]	0.89(4)	2.11(4)	2.921(4)	151(3)	x,y,z-1
	N14–H14B···O15[c]	0.83(4)	2.13(4)	2.948(3)	167(3)	x-1,y+1,z
	N15–H15···S1[d]	0.80(4)	2.47(4)	3.263(2)	173(3)	x+1,y-1,z
	C170–H17C···O15	0.96	2.15	2.823(3)	126.1	
	C21–H21A···S1	0.96	2.88	3.723(6)	146.5	
	C22A–H22B···O11	0.96	2.43	3.208(12)	137.8	
	C22B–H22E···O11	0.96	2.53	3.461(11)	162.6	
2	N11–H11···O11[a]	0.76(3)	2.12(3)	2.873(3)	177(3)	-x,-y+2,-z
	N12–H12···O11	0.77(3)	1.95(3)	2.589(3)	140(3)	
	N13–H13···O13[b]	0.92(3)	2.45(3)	3.091(3)	127(2)	-x,-y+1,-z
	N13–H13···O15[c]	0.92(3)	2.23(3)	2.993(3)	140(2)	x,-y+1/2,z+1/2
	N14–H14···O15[c]	0.85(3)	2.07(3)	2.886(3)	160(3)	x,-y+1/2,z+1/2
	N15–H15···O13[d]	0.80(3)	1.96(3)	2.738(3)	167(3)	-x,y-1/2,-z-1/2
	C170–H17B···O11[e]	0.98	2.59	3.569(3)	174.4	x,y-1,z
6•H_2O	N11–H11···O11[a]	0.91(5)	1.92(5)	2.823(6)	170(5)	-x,-y,-z+2
	N12–H12···O11	0.94(5	1.76(5)	2.551(6)	140(4)	
	N13–H13···O13[b]	0.87(5)	2.20(5)	2.948(6)	143(4)	-x+1,-y,-z+2
	N15–H15···O1[b]	0.88(5)	1.96(5)	2.839(6)	175(4)	-x+1,-y,-z+2
	O1–H1A···O15[c]	0.941(19)	1.92(3)	2.813(5)	157(5)	x-1,y,z-1
	O1–H1B···O13[a]	0.934(19)	2.05(2)	2.964(5)	165(4)	-x,-y,-z+2
	C113–H13A···N14[d]	0.99	2.68	3.548(7)	146.6	x-1/2,-y+1/2,z-1/2
	C170–H17C···O11[e]	0.98	2.39	3.343(6)	163.0	x+1,y,z

Table 3
Intermolecular $\pi\cdots\pi$ interaction parameters (Å, °) for **2** and **6**·H_2O*.

Comp.	Ring	$\pi\cdots\pi$	Cg-Cg	α	IPD	SA	Symmetry
2	N11/C11/C16/C15/N15/C13	Cg1-Cg1a	3.368	0.03	3.2602	0.847	-x, 1-y, -z
6·H_2O	N11/C11/C16/C15/N15/C13	Cg1-Cg1a	3.599	0.00	-3.2514	1.544	1-x, -y, 2-z

*CgI/CgJ are the centroids of the corresponding rings. Cg-Cg is the center-to-center distance (distance between ring centroids), α is the angle between mean planes of the rings, IPD is the mean interplanar distance (distance from one plane to the neighboring centroid) and SA is the mean slippage angle (angle subtended by the intercentroid vector to the plane normal). For details, see [37].

Å^3 that represents 33% of the volume of the unit cell and is occupied by the crystallization molecule, which is retained by the formation of some hydrogen bonds (vide infra).Thus, crystal packing in **1**·DMSO is governed by numerous hydrogen bonds (Table 2). Each Ac4NDH molecule is linked to three other nearest neighbor molecules by means of N–H···O and N–H···S hydrogen bonds (Fig. 2a), forming two heterosynthons of the $R_2^2(8)$ graph set, in which the thioamide group and an HN–C(O) group of the 2,4,6-pyrimidinetrione ring participate, generating chains parallel to the a-axis, each linked to another symmetrically related by a homosynthon of the $R_2^2(8)$ ring motif of a second HN–C(O) group, originating double chain bands (Fig. 2b). These double ribbons, which contain two N–H bonds directed outwards, form N–H···O hydrogen bonds with the oxygen atom of a DMSO molecule, causing a heterosynthon of the $R_2^1(6)$ graph set motif. Likewise, two CH bonds of both methyl groups of the same DMSO molecule participate in weak non-classical hydrogen bonds with the third oxygen atom of the 2,4,6-pyrimidinetrione ring and the thioamide sulfur atom of the corresponding TSC molecule of a new ribbon, bringing about the formation of a heterosynthon of the $R_3^2(11)$ graph set (Fig. 2c), without the splitting of the C-H bonds of the disordered methyl group significantly affect the network packing, although the corresponding geometric parameters differ slightly (Table 3). This new band is parallel to the previous one but displaced in the direction of the c-axis, so that it forms a "ladder" along the b-axis where said bands, joined by DMSO molecules, constitute the steps of the same (Fig. 3).

In the crystal packing of **2**, the presence of the methyl substituent in N14 causes a decrease in the number of N–H donors with respect to **1**·DMSO, so a lower number of classical intermolecular hydrogen bonds should be expected. Furthermore, the absence of crystallization molecules should simplify packing. In the molecule of **2**, the C11 and N12 atoms show a flat arrangement that corresponds to an S(6) N–H···O motif. In addition, each Acb4NM molecule forms intermolecular N–H···O hydrogen bonds with the five nearest neighboring molecules (Table 2), highlighting the connection between molecules by C(4) interactions that consist of N–H···O hydrogen bonds, which results in chains running along the b-axis (Fig. 4a). Similarly, an $R_1^2(6)$ heterosynthon ring motif is also formed between the N–H bonds of the hydrazine (N13) and thioamide (N14) of the thiosemicarbazone moiety as donors and the third oxygen atom of the 2,4,6-pyrimidinetrione ring (O15) as acceptor, and a classical homosynthon amide, ring motif $R_2^2(8)$, in which two HN–C(O) groups of two related centrosymmetric molecules participate (Fig. 4b). The set of the aforementioned hydrogen bonding interactions brings about a 3D network based on independent double chains parallel to the c axis (Fig. S31a in Supporting Information file). Inversion-related pairs of these chains are linked by a π–π stacking interaction; the pyrimidine rings of the molecules at (x, y, z) and (−x, 1−y, −z) are strictly parallel, with an interplanar spacing of 3.260 Å and a ring-centroid separation of 3.368 Å (Table 3 and Fig. S31b in Supporting Information file).

For the purposes of classical hydrogen bond formation, each molecule of **6**·H_2O has four donor N-H bonds and three acceptor

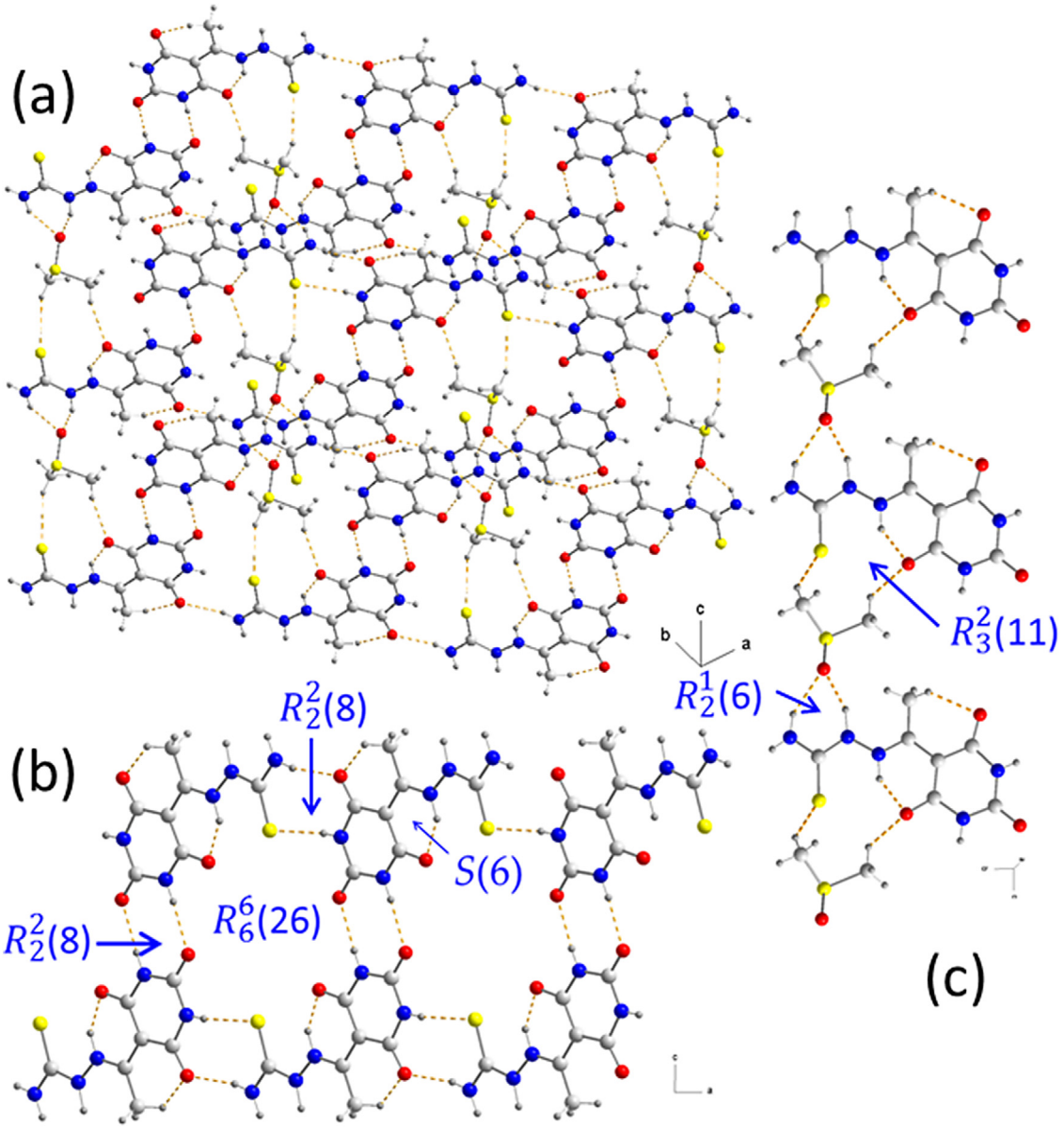

Fig. 2. Crystal packing of the molecules in **1**·DMSO, including supramolecular synthons: (a) projection on the ab-plane, (b) projection on the ac-plane, and (c) perspective view parallel to the c-axis (see Table 3).

oxygen atoms in addition to the two donor O-H and one acceptor oxygen atom of the crystallization water molecule; all of these play an important role in **6**·H_2O crystal packing, where all donors and acceptors participate (Table 2, Fig. 5). In addition to the intramolecular hydrogen bonding of graph-set $S(6)$, a structural analysis of the crystal packing reveals the presence of N-H···O bonded $R_2^2(8)$ heterosynthons between two centrosymmetrically related nearest neighboring molecules, from coordinates (x, y, z) and (−x, −y, 2−z) (Fig. 5a). Both hydrogen bonds are also present in the networks of compounds **1**·DMSO and **2**. The hydrazine nitrogen atom, N13, is committed to the carbonyl oxygen atom, O13, in the “para” position with respect to the thiosemicarbazone moiety of a new centrosymmetric molecule of **6**·H_2O, generated by the coordinates (1−x, −y, 2−z), giving rise to a new dimer of the $R_4^4(18)$ ring-motif (Fig. 5b). The intermolecular bonding in these dimers is reinforced by π-π stacking interactions between their pyrimidine rings, with an interplanar spacing of 3.251 Å and a centroid-centroid distance of 3.599 Å (Table 3, Fig. 5c). Finally, the two oxygen atoms and the NH bond of the 2,4,6-pyrimidinetrione ring, not involved in the homosynthon described above, participate in a three-centered hydrogen bond between the crystallization water molecule and three molecules of **6**·H_2O, giving rise to a homosynthon from the $R_4^2(16)$ graph-set (Fig. 5d). Ultimately, the set of all interactions gives rise to pairs of columns parallel to the c-axis formed by double molecules that are arranged mutually parallel in the crystal lattice, in the form of a zigzag according to the "bc" plane (Fig. S32 in Supporting Information file).

3.5. Hirshfeld surface analysis

We have performed a complete description of the main intermolecular interactions that are responsible for the crystal packing of compounds **1**·DMSO, **2** and, **6**·H_2O by using Hirshfeld surface analysis. Fig. 6 shows Hirshfeld surfaces mapped with the d_{norm} property, where arrows with numbers indicate close contacts. The red spots on the surfaces represent distances shorter than the sum

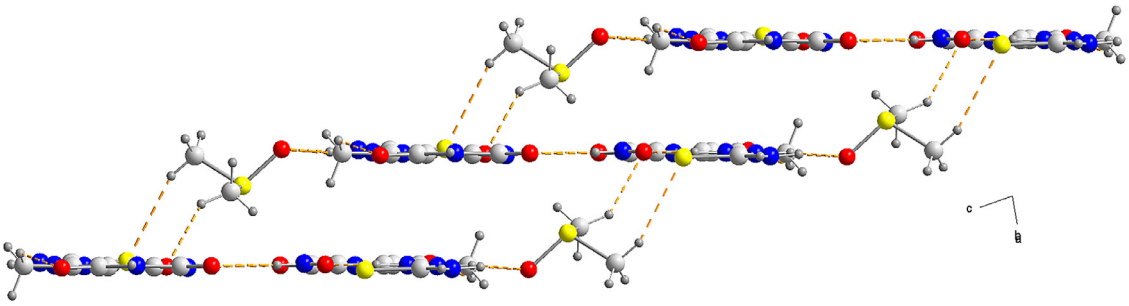

Fig. 3. Partial crystal packing in **1**·DMSO showing a ladder arrangement along the b-axis.

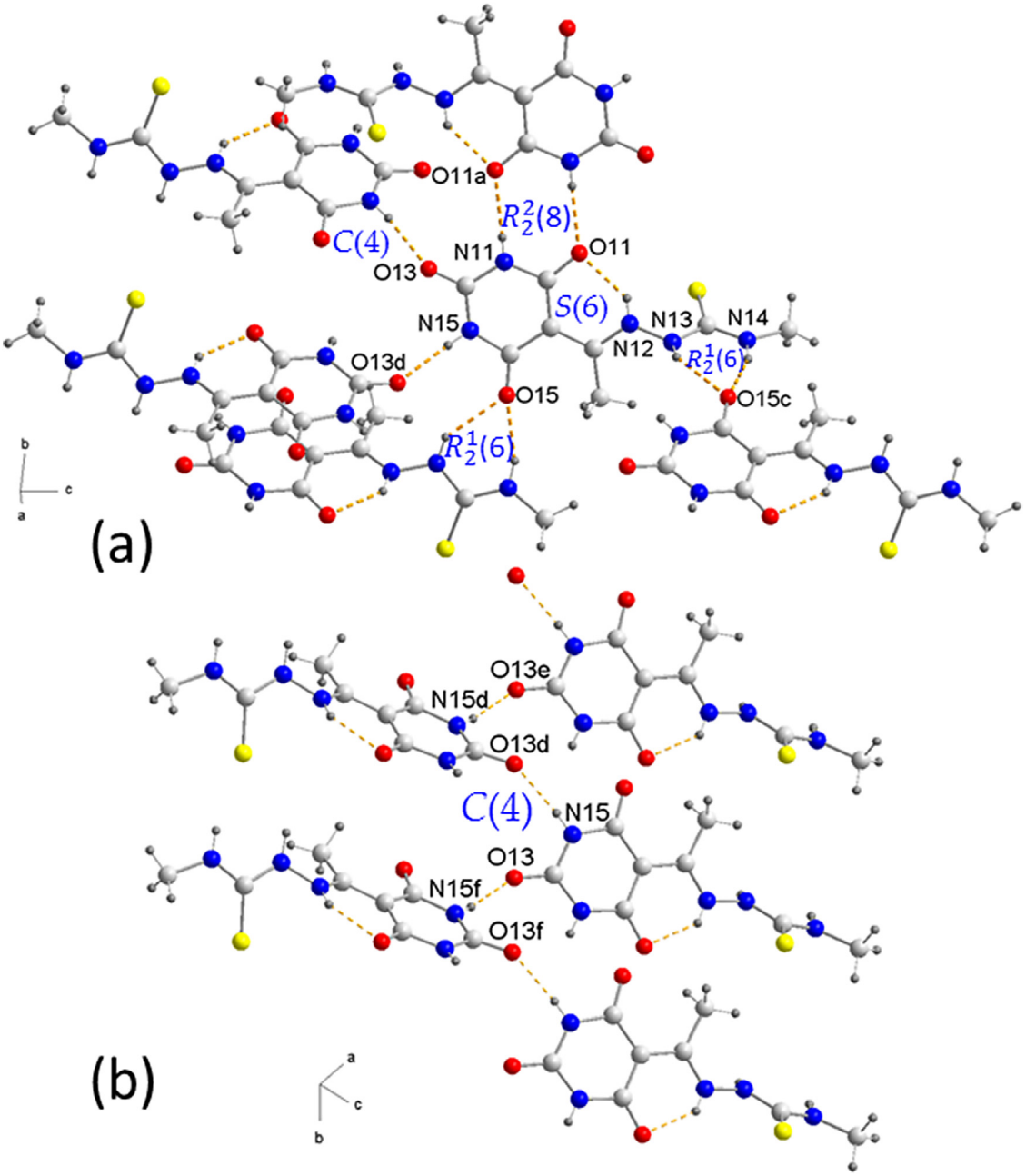

Fig. 4. (a) A partial packing diagram for **2**, showing a *C*(4) chain along the b-axis, and (b) the graph set H-bonded motifs present in the crystal structure of **2**. See Table 3 for symmetry codes.

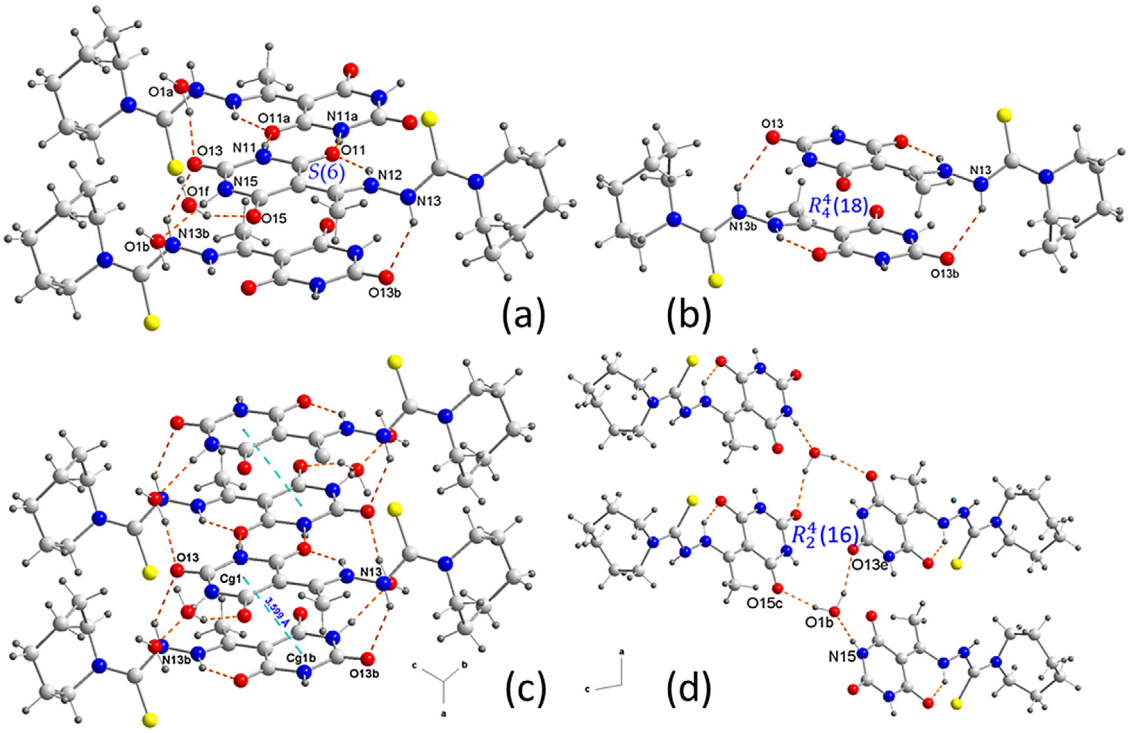

Fig. 5. (a) The intra- and intermolecular hydrogen bonds (orange dashed lines) in compound **6**·H_2O: (b) Supramolecular $R_4^4(18)$ ring in the dimer in **6**·H_2O; (c) Detail of π-π stacking interactions (blue dashed lines); (d) Supramolecular $R_2^4(16)$ ring in the tetramer in **6**·H_2O. See Tables 2 and 3 for symmetry codes.

of vdW radii and blue regions correspond to the distance longer than the sum of vdW radii. Two-dimensional (2D) fingerprint plots were obtained by calculating the distances from the Hirshfeld surface to the nearest nucleus inside the surface (d_i) and outside the surface (d_e) to analyze the molecular interactions around the nearest neighbor molecules. In 2D fingerprint plots, green regions show a higher intensity of pixels, indicating a higher frequency of contacts. Full 2D fingerprint plots of the main intermolecular contacts are depicted in Fig. 7.

In compound **1**, the large red regions labeled 1 (Fig. 6) represent H···O/O···H contacts, which are attributed to the strong N11–H11···O13 hydrogen bonds involving the H11 and O13 atoms from the 2,4,6-pyrimidinetrione moiety. The large red spots labeled 2 are associated to the N14–H14B···O15 hydrogen bonds between the amino group and the O15 atom as acceptor. In addition, the red regions labeled 4, 5 and 6 are assigned to the N13–H13···O20, N14–H14A···O20 and C22A–H22B···O11 hydrogen bonds, respectively. These H···O/O···H contacts are visible in the 2D fingerprint plot (Fig. 2) as a pair of symmetrical spikes at (d_e + d_i) ≈ 1.8 Å with a contribution of 29.5% to the total Hirshfeld surface area. The large red regions labeled 3 and 7 in the d_{norm} map are attributed to the N15–H15···S1 and C21–H21A···S1 hydrogen bonds, respectively. These interactions are also observed as sharp spikes in the fingerprint plot with a short (d_e + d_i) ≈ 2.2 Å contributing 13.6% to the total Hirshfeld surface (Fig. 7).

In compound **2**, the red regions labeled 1-5 in the d_{norm} surfaces (Fig. 6) are attributed to strong N–H···O hydrogen bonds and they are represented as a pair of longer and symmetrical spikes at (d_e + d_i) ≈ 1.75 Å in the fingerprint plot, with a high contribution of 29.5%. Like in structure **1**, the small red spots labeled 6 indicate weak C170–H17B···O11 hydrogen bonds involving the H17B atom of the methyl group and the O11 atom from the 2,4,6-pyrimidinetrione moiety. As previously deduced, the crystal packing of compound **2** is also stabilized by π-π stacking interactions between pyrimidine rings. The Hirshfeld surfaces mapped over the d_{norm} function show small red spots around the C and N atoms of the pyrimidine rings, indicating that C···C and C···N contacts are favored.

In compound **6**, the red regions labeled 1 and 2 in the d_{norm} maps are attributed to the N11–H11···O11 and N13–H13···O13 hydrogen bonds, respectively. The red spots labeled 3 are mainly assigned to N15–H15···O1 involving the O1-atom from the water molecule as acceptor. In addition, the O1–H1B···O13 and O1–H1A···O15 hydrogen bonds are visible in the d_{norm} surfaces as red spots labeled 4 and 5, respectively and represent the water H-atoms interacting with carbonyl O-atoms. These contacts are visible in the fingerprint plot (Fig. 7) as a pair of symmetrical spikes at (d_e + d_i) ≈ 1.8 Å, in accordance with the H···O distances reported in Table 3. The small red spots labeled 6 and 7 in the d_{norm} map are attributed to the C170–H17C···O11 and C13–H13A···N14 hydrogen bonds, respectively. Like in structure **2**, the red spots located around the C and N-atoms of the pyrimidine rings are indicative of π-π stacking interactions.

The Hirshfeld surface analysis also reveals that in all the studied compounds, the van der Waals H···H contacts operate in the crystal packing of all three structures. These contacts are highlighted in the middle (labeled 1) of scattered points of the fingerprint plot and contribute to the crystal stabilization in a wide range between 29.5-44.9%, as result of the relative abundances of H-atoms in the respective molecules. In addition, (de + di) sum are in the range 2.1-2.4 Å (around the sum of vdW radii), indicating the attractive nature of these contacts. Besides the aforementioned hydrogen bonds, the crystal structure of compounds 2 and 6 features a significant contribution from π-π stacking interactions (Table 3). These interactions occur between layers of pyrimidine rings (C_g1 and C_g1^a) for structures **2** and **6**. C···C contacts appear as a distinct pale blue to green area (highlighted in red) at around $d_e = d_i = 1.8$ Å in the fingerprint plots for compounds **2** and **6**, with major contributions of 3.3% for **2**. The π-π stacking interactions described previously for compounds **2** and **6** can be seen on the Hirshfeld

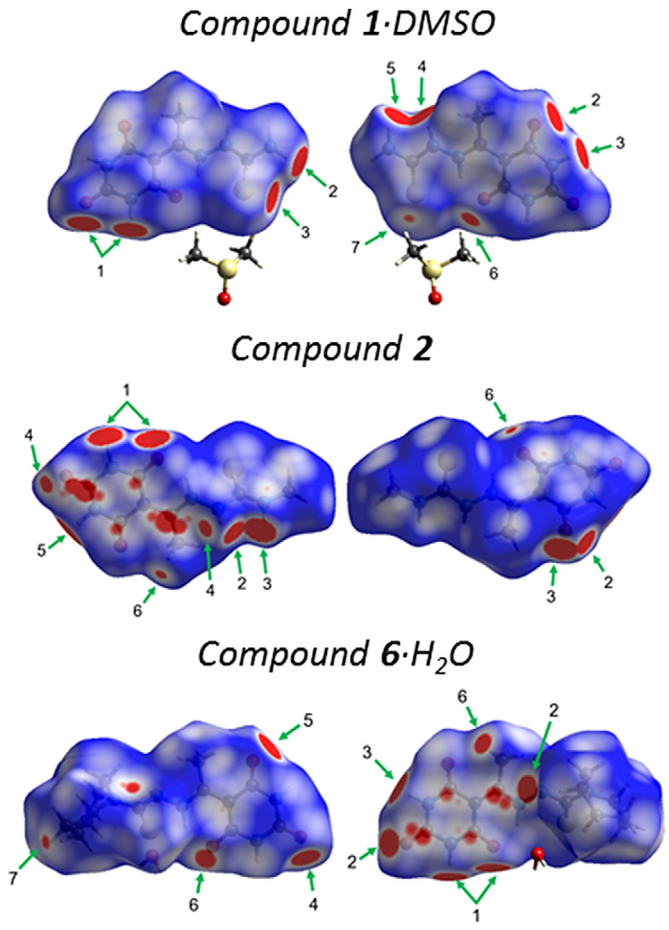

Fig. 6. Hirshfeld surfaces of compounds **1**·DMSO, **2** and 6·H_2O mapped with d_{norm} property in two orientations. The second molecule is rotated around the horizontal axis of the plot. The labels are discussed in the main text.

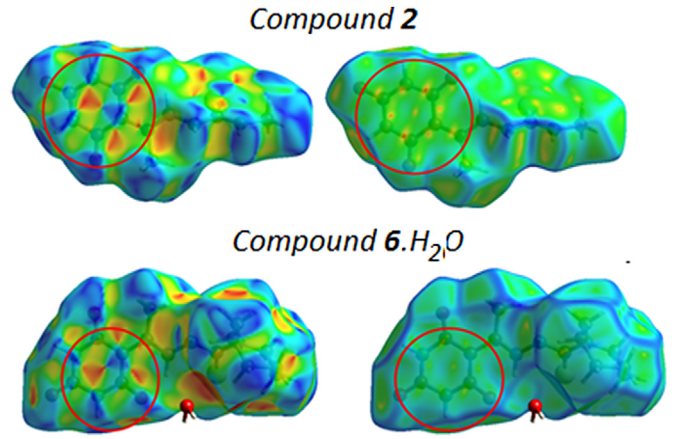

Fig. 8. Hirshfeld surfaces of compounds **2** and **6** mapped with shape index (a) and curvedness (b).

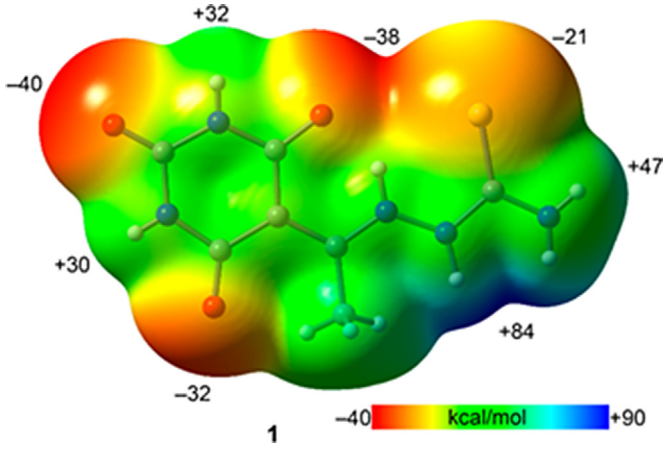

Fig. 9. Molecular electrostatic potential (MEP) surface (isosurface 0.001 a.u.) of compound **1** at the PBE0-D3/def2-TZVP level of theory. The values at selected points of the surfaces are given in kcal/mol.

surface mapped with shape index, as a pattern of alternating red and blue triangles highlighted with a red circle in Fig. 8. In addition, the curvedness surfaces clearly show large green regions on the same side of the molecules, demonstrating the presence of π-π stacking interactions.

3.6. DFT study

The theoretical DFT study is devoted to analyzing several H-bonded and π-π stacking assemblies observed in the X-ray solid state structures of compounds **1, 2** and **6**. First, the MEP surface of compound **1**, as a model of the acetylbarbituric-thiosemicarbazone hybrid, was obtained and is represented in Fig. 9. It reveals that the maximum MEP value is located in the middle of the NH groups of the thiourea moiety (+84 kcal/mol). Several local maxima are situated at the remaining N–H bonds, ranging from +30 to +48 kcal/mol. The MEP values at the N–H groups belonging to the six-membered ring are smaller than those at the thiosemicarbazone arm. The MEP minima are located in the O-atoms of the barbituric acid part of the hybrid, ranging from −32 to −40 kcal/mol, which are more negative than that at the S-atom (−21 kcal/mol).

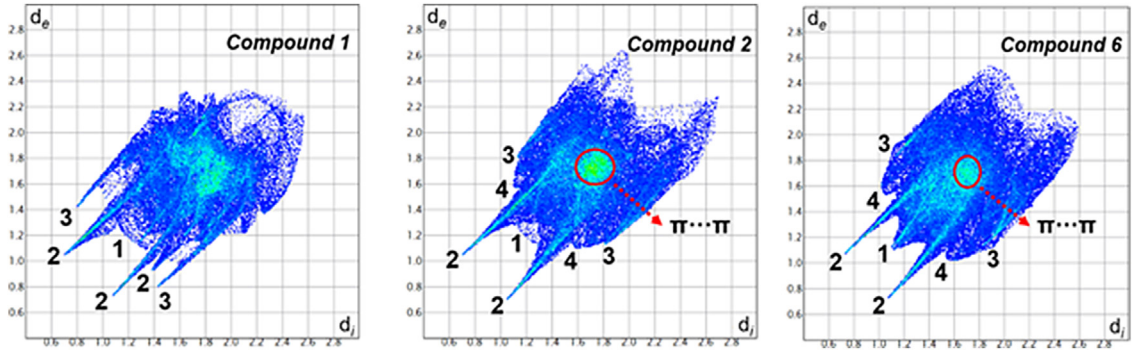

Fig. 7. Full two-dimensional fingerprint plots for compounds **1, 2** and **6**. Close contacts are labeled as follows: (1) H···H, (2) H···O/O···H, (3) H···S/S···H, (4) H···C/C···H.

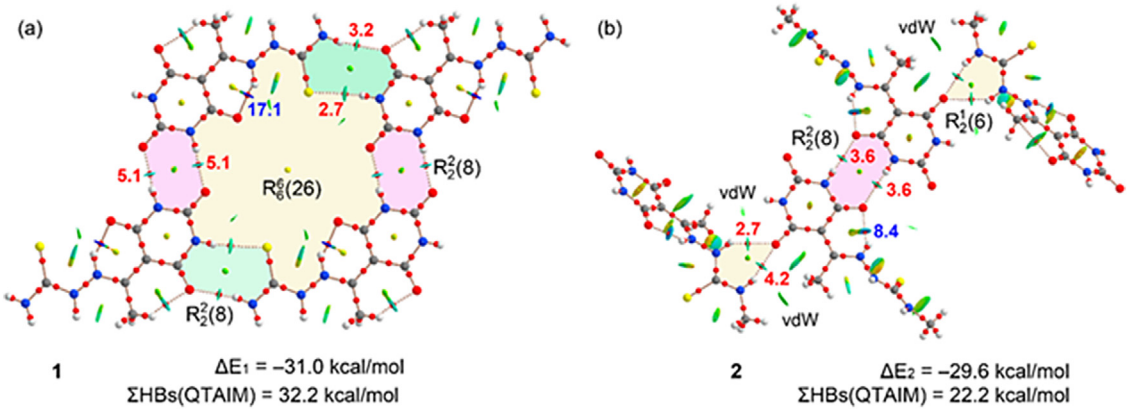

Fig. 10. Combined QTAIM/NCIplot analysis of the H-bonded tetramers of **1** (a) and **2** (b) extracted from their solid-state X-ray structure.

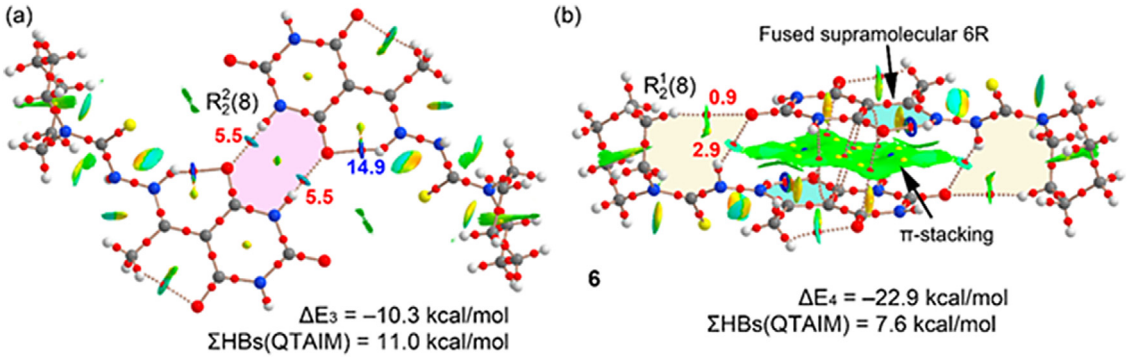

Fig. 11. Combined QTAIM/NCIplot analysis of the H-bonded (a) and π-stacked (b) dimers of **6** extracted from their solid-state X-ray structure.

This analysis reveals that **1** is very rich in H-bond donor and acceptor groups, being a better H-bond donor than acceptor.

Fig. 10 shows the QTAIM/NCIPlot analysis of the tetrameric assemblies extracted from the solid state of compounds **1** and **2**. A network of inter and intramolecular H-bonds is established, as already described above (Figs. 2b and 4b). The formation energies of the assemblies at the PBE0-D3/def2-TZVP level of theory were also computed. Moreover, the dissociation energy of each HB using the QTAIM potential energy density (V_r) predictor [38] is also indicated next to the bond CPs (in blue for intramolecular HBs and in red for intermolecular HBs). For compound **1**, in the $R_2^2(8)$ symmetric synthons (in pink), two equivalent H-bonds are formed (Fig. 10a), characterized by the corresponding bond critical points (represented as red spheres) and bond paths interconnecting the H and O-atoms. Moreover, a ring CP (yellow sphere) emerges upon complexation due to the formation of a supramolecular ring. The NCIplot analysis reveals that these H-bonds are moderately strong, since they are characterized by blue isosurfaces, which agrees well with their dissociation energy (5.1 kcal/mol). In the asymmetric $R_2^2(8)$ synthons (in green), two different H-bonds are formed, characterized by the corresponding bond CPs, and bluish NCIplot isosurfaces. The dissociation energies of the HBs of this synthon are 3.2 and 2.7 kcal/mol, thus weaker than those of the symmetric synthon, which agrees well with the MEP values shown in Fig. 9 at the different donor and acceptor groups. The QTAIM/NCIplot analysis also reveals that the intramolecular N–H···O=C is very strong (blue isosurface) with a dissociation energy of 17.1 kcal/mol. It is worth mentioning that the formation energy of the assembly is very similar (in absolute value) to the sum of the dissociation energies of the H-bonds measured using the QTAIM data at the bond CPs, thus giving reliability to the V_r energy predictor.

For compound **2**, in the symmetric $R_2^2(8)$ synthon (in pink, Fig. 10b), the HBs are characterized by the corresponding bond CPs and bond paths interconnecting the H and O-atoms. The NCIplot analysis and the dissociation energy (3.6 kcal/mol) reveals that these HBs are weaker than those observed for the symmetric synthon $R_2^2(8)$ in **1**, which is due to the participation of the O13 atom as H–bond acceptor in **1** (see Fig. 1 for atom numbering scheme), which is the most negative O-atom of the barbituric ring. In the asymmetric synthons $R_2^2(6)$ (in light yellow), two different H-bonds are formed, which are characterized by the corresponding bond CPs, and bluish isosurfaces. The dissociation energies of the HBs of this synthon are 4.2 and 2.7 kcal/mol, one of which is stronger than those of the symmetric synthon. The formation energy of the assembly is greater (in absolute value) that the sum of the dissociation energies of the H-bonds, thus revealing the existence of additional vdW interactions that also contribute to the stabilization of the assembly. In fact, several green isosurfaces are located between the monomers (marked as vdW in Fig. 10b), supporting this explanation. This fact was also observed in the Hirshfeld surface analysis mentioned above.

Fig. 11 shows the self-assembled dimers analyzed for compound **6**, described in Fig. 5a and 5b. In the H-bonded dimer (Fig. 11a), the symmetric synthon $R_2^2(8)$, already described for **1** and **2** is analyzed. The H-bonds are stronger for this compound, compared to **1** and **2**, in agreement with the shorter experimental distances. Again, the sum of the HB dissociation energies agrees very well with the formation energy of the assembly, thus validating the QTAIM predictor. In the π-stacked dimer (Fig. 11b), an intricate combination of interactions is observed, that likely explain the large dimerization energy (ΔE_4 = –22.9 kcal/mol). The contribution of the H-bonds is 7.6 kcal/mol from the symmetric synthons $R_2^2(8)$. The rest of the dimerization energy comes from the π-stacking where the most intriguing observation is that the supramolecular 6-membered ring (OCCCNH) also participates in the binding mode given that it is stacked over the barbituric ring.

In fact, the large NCIplot isosurface embraces both the barbituric acid and the fused 6-membered supramolecular ring (highlighted in light blue in Fig. 11b).

4. Conclusions

Six new 5-acetylbarbituric-thiosemicarbazone derivatives (**1** to **6**) have been synthesized, with yields of 60-80%, using a relatively easy method based on a three-component, one-pot acid-catalyzed reaction, and then spectroscopically characterized. A seventh compound has also been unexpectedly obtained from the reagents involved in the synthesis of **1** and a plausible mechanism for its formation has been proposed. The molecular and crystal structure of three thiosemicarbazones (**1**·DMSO, **2,** and **6**·H_2O) were also determined by single crystal X-ray crystallography, and an exhaustive analysis of their supramolecular structures has been carried out. The energetic features of the assemblies have been analyzed using DFT calculations and the individual contribution of each H-bond has been estimated using the V_r value at the bond CP. The energetic study reveals that the π-stacking assemblies are very relevant energetically thus confirming their importance in the crystal packing. The QTAIM/NCIplot analyses reveal that the H-bonded supramolecular ring also participates in the π-stacking binding mode, further contributing to the formation of highly stable supramolecular dimers.

Credit author statement

I am giving work contribution in "Supramolecular, spectroscopic and computational analysis of weak interactions in some thiosemicarbazones derived from 5-acetylbarbituric acid" by all authors. Credits of all authors are as given:

1. Alfonso Castiñeiras: Conceptualization, Methodology, Single crystal data analysis, Manuscript writing and all analysis.
2. Nuria Fernández-Hermida: He has synthesized and characterized all the compounds.
3. Isabel García-Santos: He helped in single crystal data analysis and has done supplementary data preparation.
4. Lourdes Gómez-Rodríguez: He helped in synthesis, crystallization and characterization.
5. Diego M. Gil: He has done Hirshfeld calculation.
6. Antonio Frontera: He has done DFT calculations.

Declaration of competing interest

The authors declare that they have no known competing financial interests or personal relationships that could have appeared to influence the work reported in this paper.

Acknowledgements

Financial support from the Network of Excellence "Metallic Ions in Biological Systems" CTQ2017-90802-REDT [Ministerio de Economía y Competitividad (Spain) and European Regional Development Fund (EU)], and the Xunta de Galicia (Spain) [Rede de Excelencia MetalBIO ED431D 2017/01]. MICIU/AEI of Spain (project CTQ2017-85821-R FEDER) is also acknowledged for financial support.

Supplementary materials

Supplementary material associated with this article can be found, in the online version, at doi:10.1016/j.molstruc.2021.131031.

References

[1] A. Castiñeiras, I. García-Santos, S. Nogueiras, I. Rodríguez-González, R. Rodríguez-Riobo, J. Mol. Struct. 1074 (2014) 1–18, doi:10.1016/j.molstruc.2014.05.042.
[2] H. Beraldo, D. Gambino, Mini-Rev. Med. Chem. 4 (2004) 31–39, doi:10.2174/1389557043487484.
[3] B.M. Paterson, P.S. Donnelly, Chem. Soc. Rev. 40 (2011) 3005–3018, doi:10.1039/C0CS00215A.
[4] P.J. van Koningsbruggen, J.G. Haasnoot, R.A.G. de Graaff, J. Reedijk, Inorg. Chim. Acta 234 (1995) 87–94, doi:10.1016/0020-1693(95)04487-T.
[5] A. Sharma, Y. Jad, M.R.H. Siddiqui, B.G. de la Torre, F. Albericio, A. El-Faham, J. Chem. (2017) 10 ID 5702962, doi:10.1155/2017/5702962.
[6] E. Bermejo, A. Castiñeiras, I. García-Santos, L. Gómez-Rodríguez, P. Sevillano, Z. Anorg. Allg. Chem. 633 (2007) 2255–2261, doi:10.1002/zaac.200700151.
[7] H. Biltz, H. Wittek, Chem. Ber. 54 (1921) 1035–1058, doi:10.1002/cber.19210540519.
[8] A.C.T. North, D.C. Phillips, F.S. Mathews, Acta Crystallogr. A24 (1968) 351–359, doi:10.1107/S0567739468000707.
[9] G.M. Sheldrick, SADABS, Program for Empirical Absorption Correction of Area Detector Data, University of Göttingen, Germany, 2001 https://cmacd.myweb.cs.uwindsor.ca/Teaching/553-class/sadabs.pdf.
[10] G.M. Sheldrick, Acta Crystallogr. A71 (2015) 3–8, doi:10.1107/S2053273314026370.
[11] H. Putz, K. Brandenburg, DIAMOND - Crystal and Molecular Structure Visualization Version 4.6.2, Crystal Impact GbR, Bonn, Germany, 2020 https://www.crystalimpact.com/diamond/.
[12] J.J. McKinnon, M. Spackman, A.S. Mitchel, Acta Crystallogr. B60 (2004) 627–668, doi:10.1107/S0108768104020300.
[13] Y.H. Luo, C. Chen, D.L. Hong, X.T. He, J.W. Wang, B.W. Sun, J. Phys. Chem. Lett. 9 (2018) 2158–2163, doi:10.1021/acs.jpclett.8b00597.
[14] J.J. McKinnon, D. Jayatilaka, M.A. Spackman, Chem. Commun. (2007) 3814–3816, doi:10.1039/B704980C.
[15] M.A. Spackman, D. Jayatilaka, CrystEngComm 11 (2009) 19–32, doi:10.1039/B818330A.
[16] M.A. Spackman, Chem. Rev. 92 (1992) 1769–1797, doi:10.1021/cr00016a005.
[17] M.J. Turner, J.J. McKinnon, S.K. Wolf, D.J. Grimwood, P.R. Spackman, D. Jayatilaka, M.A. Spackman, Crystal Explorer 17, University of Western Australia, Perth, 2017 https://hirshfeldsurface.net.
[18] M.J. Frisch, G.W. Trucks, H.B. Schlegel, G.E. Scuseria, M.A. Robb, J.R. Cheeseman, G. Scalmani, V. Barone, G.A. Petersson, H. Nakatsuji, X. Li, M. Caricato, A.V. Marenich, J. Bloino, B.G. Janesko, R. Gomperts, B. Mennucci, H.P. Hratchian, J.V. Ortiz, A.F. Izmaylov, J.L. Sonnenberg, D. Williams-Young, F. Ding, F. Lipparini, F. Egidi, J. Goings, B. Peng, A. Petrone, T. Henderson, D. Ranasinghe, V.G. Zakrzewski, J. Gao, N. Rega, G. Zheng, W. Liang, M. Hada, M. Ehara, K. Toyota, R. Fukuda, J. Hasegawa, M. Ishida, T. Nakajima, Y. Honda, O. Kitao, H. Nakai, T. Vreven, K. Throssell, J.A. Montgomery Jr., J.E. Peralta, F. Ogliaro, M.J. Bearpark, J.J. Heyd, E.N. Brothers, K.N. Kudin, V.N. Staroverov, T.A. Keith, R. Kobayashi, J. Normand, K. Raghavachari, A.P. Rendell, J.C. Burant, S.S. Iyengar, J. Tomasi, M. Cossi, J.M. Millam, M. Klene, C. Adamo, R. Cammi, J.W. Ochterski, R.L. Martin, K. Morokuma, O. Farkas, J.B. Foresman, D.J. Fox, Gaussian 16, Revision B.01, Gaussian Inc., Wallingford CT, 2016 https://gaussian.com/g09citation/.
[19] S.F. Boys, F. Bernardi, J. Mol. Phys. 19 (1970) 553–566, doi:10.1080/00268977000101561.
[20] S. Grimme, J. Antony, S. Ehrlich, H. Krieg, J. Chem. Phys. 132 (2010) 154104–154118, doi:10.1063/1.3382344.
[21] A. Das, S.R. Choudhury, B. Dey, S.K. Yalamanchili, M. Helliwell, P. Gamez, S. Mukhopadhyay, C. Estarellas, A. Frontera, J. Phys. Chem. B 114 (2010) 4998–5009, doi:10.1021/jp911884x.
[22] C. Verdugo-Escamilla, C. Alarcón-Payer, A. Frontera, F.J. Acebedo-Martínez, A. Domínguez-Martín, J. Gómez-Morales, D. Choquesillo-Lazarte, Crystals 10 (2020) 1088, doi:10.3390/cryst10121088.
[23] R.F.W. Bader, Chem. Rev. 91 (1991) 893–928, doi:10.1021/cr00005a013.
[24] J. Contreras-García, E.R. Johnson, S. Keinan, R. Chaudret, J.-P. Piquemal, D.N. Beratan, W. Yang, J. Chem. Theor. Comput. 7 (2011) 625–632, doi:10.1021/ct100641a.
[25] A. Keith, AIMAll (Version 19.02.13), TK Gristmill Software, Overland Park KS, USA, 2019. http://aim.tkgristmill.com
[26] E. Bermejo, A. Castiñeiras, R. Domínguez, R. Carballo, C. Maichle-Mössmer, J. Strähle, D.X. West, Z. Anorg. Allg. Chem. 625 (1999) 961–968 10.1002/(SICI)1521-3749(199906)625:6≤961::AID-ZAAC961≥3.0.CO;2-J.
[27] T. Bamgboye, O.A. Bamgboye, Inorg. Chim. Acta 105 (1985) 223–226, doi:10.1016/S0020-1693(00)85235-4.
[28] R.A. Rusell, H.W.M. Thomson, Spectrochim. Acta 8 (1956) 136–141, doi:10.1016/0371-1951(56)80049-0.
[29] M.A. Ali, K. Dey, M. Nazimuddin, F.E. Smith, R.J. Butcher, J.P. Jasinski, J.M. Jasinski, Polyhedron 15 (1996) 3331–3339, doi:10.1016/0277-5387(96)00003-4.
[30] D.S. Mahadevappa, A.S.A. Murthy, Aust. J. Chem. 25 (1972) 1565–1568, doi:10.1071/CH9721565.
[31] B.S. Jursic, D.M. Neumann, Tetrahedron. Lett. 42 (2001) 8435–8439, doi:10.1016/S0040-4039(01)01830-5.
[32] (a) D.X. West, H. Gebremedhin, T.J. Romac, A.E. Liberta, Transit. Met. Chem. 19 (1994) 426–431, doi:10.1007/BF00139320; (b) D.X. West, G.A. Bain, R.J. Butcher, J.P. Jasinski, Y. Li, R.Y. Pozdniakiv, J. Valdés-Martínez, R.A. Toscano, S. Hernández-Ortega, Polyhedron 15 (1996) 665–674, doi:10.1016/0277-5387(95)00298-7.

[33] J.T. Bojarski, J.L. Mokrosz, H.J. Bartón, M.H. Paluchowska, Adv. Heterocycl Chem. 38 (1985) 229–297, doi:10.1016/S0065-2725(08)60921-6.
[34] K. Ohui, E. Afanasenko, F. Bacher, R. Lim Xue Ting, Z. Ayesha, N. Blanco-Cabra, E. Torrents, O. Dömötör, N.V. May, D. Darvasiova, É.A. Enyedy, A. Popović-Bijelić, J. Reynisson, P. Rapta, M.V. Babak, G. Pastorin, V.B. Arion, J. Med. Chem. 62 (2019) 512–530, doi:10.1021/acs.jmedchem.8b01031.
[35] A. Olczak, M.L. Główka, J. Gołka, M. Szczesio, J. Bojarska, K. Kozłowska, H. Foks, C. Orlewska, J. Mol. Struct. 830 (2007) 171–175, doi:10.1016/j.molstruc.2006.07.011.
[36] T.C. Lewis, D.A. Tocher, S.L. Price, Cryst. Growth. Des. 4 (2004) 979–987, doi:10.1021/cg034209a.
[37] C. Janiak, J. Chem. Soc., Dalton Trans. (2000) 3885–3896, doi:10.1039/B003010O.
[38] E. Espinosa, E. Molins, C. Lecomte, Chem. Phys. Lett. 285 (1998) 170–173, doi:10.1016/S0009-2614(98)00036-0.